Normal and shear forces between boundary sphingomyelin layers under aqueous conditions

Normal and Shear Forces between Boundary Sphingomyelin Layers under Aqueous Conditions

Yifeng Cao, Nir Kampf, Weifeng Lin, and Jacob Klein*

Department of Materials and Interfaces, Weizmann Institute of Science, Rehovot 76100, Israel

*Jacob.klein@weizmann.ac.il

Abstract

Sphingomyelin is one of the predominant phospholipid groups in synovial joints, where lipids have been strongly implicated in the boundary lubrication of articular cartilage; however, little attention has been paid to its lubrication behavior. In this study, we demonstrate that sphingomyelin is an excellent boundary lubricant by measuring the normal and shear forces between sphingomyelin-layer-coated surfaces with a surface force balance under aqueous conditions. Slightly negatively-charged egg sphingomyelin vesicles were adsorbed on mica either by calcium bridging or by charge screening with high concentration monovalent salt. The normal force profiles between opposing egg sphingomyelin layers (vesicles or bilayers) show long-ranged weak repulsion and short-ranged strong repulsion on approaching. Friction coefficients, calculated from the highest load, were $(7.2 \pm 1.7) \times 10^{-4}$ at contact stresses of 9.1 ± 0.7 across 0.3 mM liposome dispersion in 0.03 mM Ca^{2+}, and $(0.8 - 3.5) \times 10^{-3}$ at contact stresses of 7.6 ± 0.8 MPa across 0.3 mM liposome dispersion in 150 mM $NaNO_3$. Similar or slightly lower friction coefficients of $(5.3 \pm 0.8) \times 10^{-4}$ at 9.8 ± 0.2 MPa were obtained by replacing the liposome dispersion in 0.03 mM Ca^{2+} by water. Such low friction coefficients, attributed to the hydration lubrication mechanism, are comparable to those of phosphatidylcholine lipids, which have been widely recognized as excellent aqueous biolubricants. Therefore, we believe that sphingomyelin, in parallel with phosphatidylcholine, contributes to the remarkably good boundary lubrication in synovial joints.

Keywords: sphingomyelin, hydration lubrication, surface forces, friction coefficient, boundary lubricant.

Introduction

The identification and characterization of lubricants from biolubrication systems leads to better understanding the superlubrication mechanisms (where superlubricity is commonly defined as a friction coefficient $\mu < 0.01$)[1] and designing efficient lubricants and wear protectors. Synovial joints, such as hips and knees, are capable of providing extremely low friction coefficients down to $0.03 - 0.001$[2, 3] under a wide range of physiological pressures (up to 4 – 18 MPa),[4-7] and thus have been attracting particular attention. Certain major molecular constituents of synovial joints, especially phosphatidylcholine (PC) lipids, have been investigated as potential boundary lubricants.[8-10] PCs are the most abundant phospholipid (PL) class in synovial joints and the most extensively studied PLs. By themselves or when complexed with hyaluronic acid, PCs in model experiments exhibit comparable or even superior lubrication performance to biolubrication systems, attributed to the hydration lubrication paradigm.[11-14]

PLs identified in synovial joints comprise different headgroup structures and hydrocarbon chain lengths and degrees of unsaturation.[15, 16] Next to PC, sphingomyelin (SM) is the most abundant PL, accounting for ca. 17% in human synovial fluid[16] and 32% on bovine cartilage surface[15]. In addition, it is also a major component of eukaryotic cell membrane[17] and ocular lens membranes[18]. The chemical structure of SM (Figure 1a) consists of a sphingosine moiety, a phosphocholine headgroup, and a fatty acid chain. Both SM and PC have a phosphocholine headgroup and two hydrophobic tails, and their structural difference mainly lies in the interfacial part: the glycerol-based PC molecule has two ester bonds,

which act only as hydrogen-bond acceptors; while SM lipid bears a hydroxyl and an amide group, which are capable of both accepting and donating hydrogen-bond.

This structure of SM lipids influences their properties and behavior. Compared with PCs, SM molecules form more complicated intra- and inter-molecular hydrogen-bonds within the SM bilayer, giving rise to differing physiological properties. The SM molecules in a bilayer show more ordered packed tails, smaller area per lipid, and slightly lower hydration levels, together with higher Young's modulus and bending modulus of the bilayer.[19-22] Moreover, SM molecules form specific hydrogen-bonding interactions with co-lipids.[23] Together with cholesterol, SM plays a key role in constituting "raft" structures on plasma cell membranes, interacting with functional proteins and being involved in many essential biological functions, such as cellular signaling and ion channel regulation.[17, 24, 25]

Due to the structural and biological significance of SM lipids in biological systems, particularly their potential as boundary lubricants, it is important to know the surface forces, including both normal and shear forces, between SM bilayers at physiologically high pressures. Knowledge on interactions between single-component PLs can also contribute to the studies of multi-component PL mixtures. However, except for a few studies on the hydration forces between SM bilayers[26, 27] and a macroscopic study on friction reduction ability of SM in air,[8] there is little information to date on the interactive forces and lubrication behavior under aqueous environment.

In this study, we measure the normal and shear forces between mica surfaces coated with SM small unilamellar vesicles (SUVs) using a surface force balance (SFB, Figure 1b) and elucidate the lubrication behavior of SM in aqueous media, including water and physiologically high salt solution. While such model studies cannot replicate in-vivo physiological conditions precisely, nonetheless they provide insight as to the boundary lubrication offered by the SM, as this involves energy dissipation processes at the SM surface which are likely to be similar whenever SM layers slide past each other. Since C16:0 is the predominant alkyl chain (38 – 44%) of SM molecules identified in human synovial fluid,[28] egg sphingomyelin (egg SM) containing 86% C16:0 SM was used as a model SM system for this study.

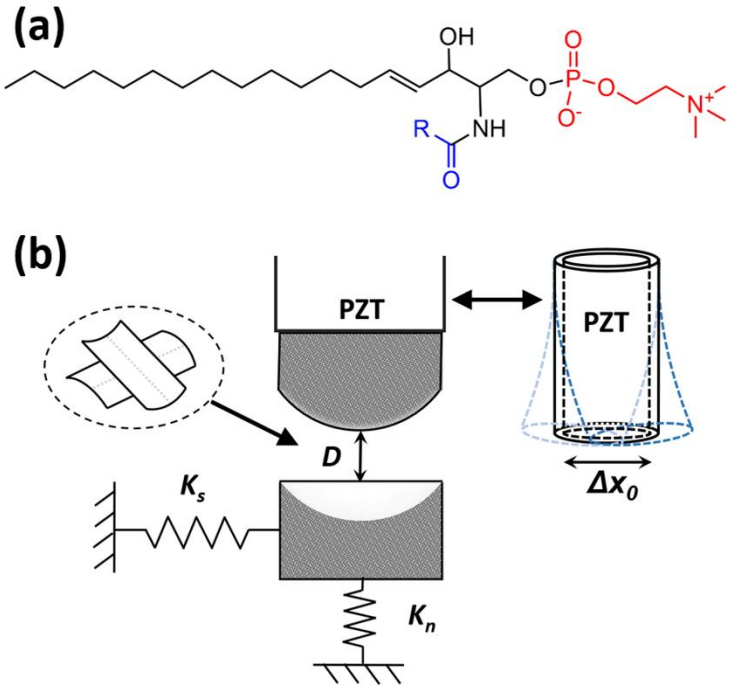

Figure 1. Chemical structure of sphingomyelin (a) and schematic illustration of SFB setup (b). A sphingomyelin molecule (a) contains a sphingosine moiety (in black), a phosphocholine headgroup (in red), and a fatty acid chain (in blue). The fatty acid composition of egg sphingomyelin used in this study consists of 86% C16:0, 6% C18:0, 3%

C22:0, 3% C24:1, and 2% unknown compounds.[29] In the SFB setup (b), two back-silvered mica facets are glued separately to two cylindrical quartz lenses in a crossed-cylinder configuration as indicated in the dashed circle, D is the closest separation distance between the mica surfaces, K_s and K_n are respectively shear and normal spring constants, and Δx_0 is the applied lateral motion of the upper lens, which is connected to the PZT.[30] (For interpretation of the references to color in this figure legend, the reader is referred to the web version of this article.)

Experimental section

Materials. Egg SM powder (purity > 99%, average molecular weight 710.965) was purchased from Avanti Polar Lipids, Inc. (Alabama, USA). Sodium nitrate ($NaNO_3$) 99.99 Suprapur® and calcium nitrate tetrahydrate ($Ca(NO_3)_2 \cdot 4H_2O$) 99.95 Suprapur® were purchased from Merk KGaA (Darmstadt, Germany). Conductivity water with a resistivity of 18.2 mΩ·cm at room temperature and total organic carbon content of ≤ 2 ppb was obtained through a Barnstead™ Nanopure™ Diamond UV/UF system (Dubuque, IA, USA).

Liposome preparation. Liposomes were prepared by the hydration-extrusion method as follows. Egg SM powder was suspended either in water or in 150 mM $NaNO_3$ aqueous solution with an initial lipid concentration of 6 mM. The suspension was sonicated in a bath sonicator at 65 °C, above the phase transition temperature of egg SM (38.1 °C by DSC),[31] for ca. 15 min with periodic vortex-mixing to obtain a homogeneous dispersion of multilamellar vesicles (MLVs). SUVs were prepared by extruding the MLV dispersion subsequently through polycarbonate membranes with pore sizes of 400, 100, and 50 nm for 5, 8, and 12 times, respectively. The temperature of the extruder chamber was controlled at 65 ± 1 °C using a water circulation bath. Extrusion was carried out inside a clean lamellar

flow hood to avoid contamination. The prepared liposome dispersion was cooled down to room temperature and stored at 4 ^{o}C before use.

Dynamic light scattering (DLS). Size distribution and zeta-potential of the liposomes were measured on a Malvern Zetasizer Nano ZSP (Worcestershire, UK). Measurements on size distribution were carried out with a backscatter angle of 173^{o} and temperature set at 25 ^{o}C. Zeta-potential was calculated automatically from the electrophoretic mobility of liposomes based on the Smoluchowski equation. Egg SM concentration at 0.3 mM was used for all the DLS measurements. Unless specified, the prepared SUV dispersions (egg SM concentration ca. 6 mM) were diluted 20-fold with the same dispersion media. For zeta potential measurements of egg SM vesicles prepared in 150 mM $NaNO_3$, the prepared SUV dispersion was diluted 2-fold with 150 mM $NaNO_3$ and then 10-fold with pure water.

Differential scanning calorimetry (DSC). Phase transition temperature of egg SM-SUVs in water was tested on a Q200 differential scanning calorimeter by TA Instruments (New Castle, DE, USA), with temperature ranging from 20 – 60 ^{o}C and at a heating/cooling rate of 0.5 ^{o}C min^{-1}.

Atomic force microscopy (AFM) imaging. AFM imaging was carried out using an Asylum MFP 3D^{TM} atomic force microscope (Santa Barbara, CA, USA). Samples were prepared by adding 0.3 mM liposome dispersions to a petri dish with a freshly cleaved mica sheet glued on the inner bottom surface. Silicon tips on a Silicon Nitride cantilever

(Bruker, model SNL-10, Santa Barbara, CA, USA) were used to scan samples via non-contact mode under 0.3 mM liposome dispersion at room temperature.

SFB measurements. The SFB setup (Figure 1b) and the measurement procedures have been described previously in detail.[30] Briefly, back-silvered mica facets (thickness ~ 2.5 μm) were glued on hemicylindrical quartz lenses with mean radius of curvature 10 mm. Two lenses glued with mica facets were amounted to SFB in a relative crossed-cylinder orientation as shown in Figure 1b. The closest separation between two mica surfaces (D) with an accuracy of ± 2 – 3 Å was determined according to the wavelength of fringes of equal chromatic order (FECO). Normal forces (F_n) were measured from the bending ($\Delta D_0 - \Delta D$) of the horizontal-spring (Figure 1b) where ΔD_0 is the applied normal motion and ΔD is the corresponding change in surface separation, so that $\Delta F_n = K_n \cdot (\Delta D_0 - \Delta D)$, where K_n is the horizontal-spring constant. Shear forces (F_s) were measured by monitoring the bending Δx of the vertical-spring (Figure 1b) with a parallel air-gap capacitor, while applying a lateral back-and-forth motion (Δx_0) via the piezoelectric tube (PZT, Figure 1b), $F_s = K_s \cdot \Delta x$, where K_s is the vertical-spring constant. Noise level of the shear force ($F_{s,0}$), induced by the mechanical vibration of the system, was recorded at $D \geq 500$ nm, where there is no shear force between two surfaces.

For liposomes prepared in water, force profiles were recorded with the mica surfaces immersed under three consecutive conditions: in 0.3 mM egg SM-SUVs liposome dispersion in water; in the liposome dispersion with 0.03 mM Ca^{2+} added ([egg SM-SUVs + Ca^{2+}]); and following the replacement of the [egg SM-SUVs + Ca^{2+}] by pure water. 0.8

mL of 6 mM egg SM-SUVs prepared in water and 0.48 mL of 1 mM $Ca(NO_3)_2$ aqueous solution were separately introduced to SFB boat (volume ca. 16 mL) to achieve the required liposome and calcium concentrations. For measurements under physiological salt concentration, 0.8 mL of 6 mM egg SM-SUVs prepared in 150 mM $NaNO_3$ was introduced to the boat filled with 150 mM $NaNO_3$ solution. Temperature was kept constant at 25 ± 1 ^oC. All the measurements were performed following equilibration for at least two hours. At least two independent experiments were carried out for each configuration.

All glassware used in the SFB experiment was cleaned with Piranha solution of 98% H_2SO_4:30% H_2O_2 ≈ 3:1 by volume (*warning*: Piranha solution is a strong oxidizing agent and should be handled with extreme care!) and the stainless tools were passivated with 15% HNO_3, followed by repeated rinsing with conductivity water to remove the chemical residuals.

Results and Discussion

Characterization of egg SM-SUVs in dispersion and on mica surface

The main phase transition temperature for egg SM-SUVs in water is determined to be 38.9 and 38.1 ^oC upon heating and cooling, respectively (Figure S1), in line with previously reported data obtained by DSC (38.1 ^oC)[31] and X-ray scattering (38.3 ^oC)[32]. Studies have assigned the T_m of egg SM as ripple gel-to-liquid phase transition.[32, 33]

Liposomes prepared from egg SM lipid dispersed in water show average size of 65.0 ± 0.62 nm (PDI 0.021) and negative zeta potential value of -12.7 ± 1.92 mV. A reduced zeta

potential was observed for liposomes prepared in $NaNO_3$ solution (-3.64 ± 0.634 mV, measured after diluting to 15 mM $NaNO_3$), possibly resulting from salt screening and specific ion adsorption.[34] Considering sphingomyelin lipid is electroneutral (Figure 1a) and egg SM is a mixture containing unknown components, the negative potential of electrical double layer surrounding the vesicles might be due to dipole orientation of zwitterionic headgroups, or impurities, or both.[35] Similarly, negative zeta potential values were reported for egg SM liposomal membrane at pH > 4 under 0.155 M NaCl[36] and milk SM liposome (155.3 ± 0.46 nm in diameter) in water (-11.4 mV)[37]. Since negatively charged mica was used as the substrate in the SFB experiments, 0.03 mM calcium was used to attach the egg SM-SUVs to the mica surface via charge bridging: calcium is a divalent cation participating in various biological activities and is found in cartilage and synovial fluid,[38, 39]. 0.03 mM calcium can largely neutralize the liposome surface charge (zeta potential -3.70 ± 0.114 mV, Figure S2), while avoiding the dehydration effect of high concentration calcium on egg SM bilayer.[40]

The morphologies of egg SM-SUVs adsorbed on mica in the presence of 0.03 mM $Ca(NO_3)_2$ and 150 mM $NaNO_3$ are shown in Figure 2. Under both conditions, we can clearly see that egg SM vesicles adsorbed and some ruptured, with a high coverage bottom layer on mica. In the presence of divalent Ca^{2+}, more intact vesicles were observed and the bottom layer is composed of closely packed round patches (Figure 2a). In 150 mM $NaNO_3$, the binding is via weaker nonspecific interactions, and some defects were observed on the bottom bilayer (Figure 2b).

Based on these results, we measured the normal and shear forces between mica surfaces coated by egg SM-SUVs/bilayer to evaluate their lubricating ability, under the following conditions. In one configuration, a 0.3 mM SUV dispersion was prepared in water and incubated with the mica surfaces; 0.03 mM Ca^{2+} was then added; finally, the bulk solution was replaced by water. In the other configuration, a 0.3 mM SUV dispersion was prepared in 150 mM $NaNO_3$, and force measurements were carried out following incubation of the mica surfaces with 0.3 mM SUVs in 150 mM $NaNO_3$.

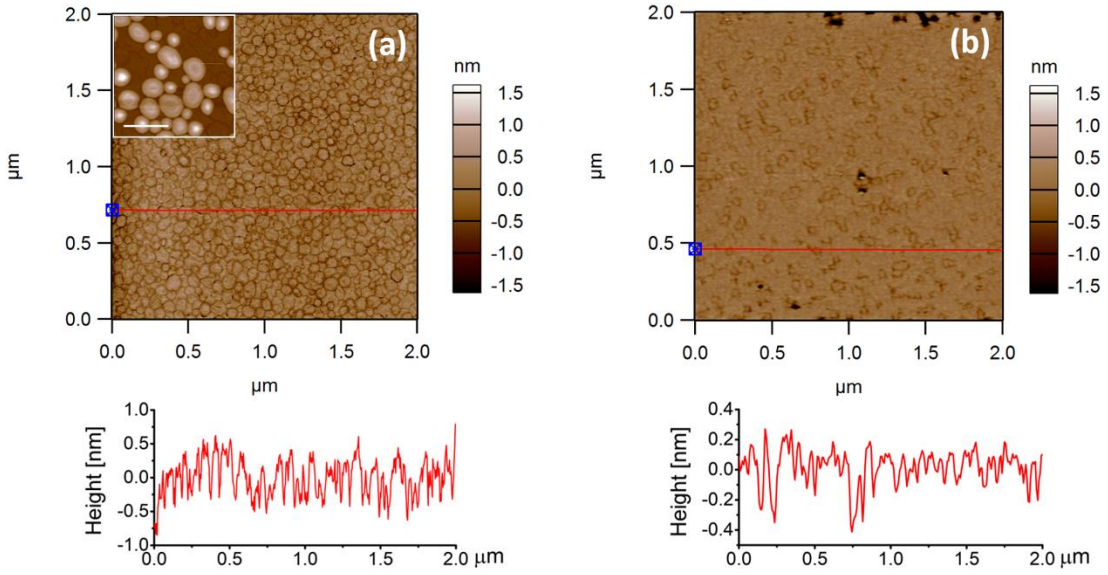

Figure 2. AFM images of egg SM-SUVs adsorbed on mica under 0.03 mM $Ca(NO_3)_2$ (a) and 150 mM $NaNO_3$ (b). Inset in (a) shows some intact egg SM-SUVs on mica when scanned with a smaller set-point, where a lower force was applied to the surface and less vesicles were ruptured by the tip. The surface roughness of the closely packed bottom layer is ca. 0.35 and 0.25 nm for (a) and (b). All the scanning was performed under 0.3 mM liposome dispersion. The scale bar in the inset of (a) is 200 nm.

Normal Force Profiles

Profiles of normalized normal forces versus separation distances (F_n/R vs. D) between egg SM layers are presented in Figures 3–5. Figures 3–4 show normal force profiles across 0.3

mM egg SM-SUVs before and after adding 0.03 mM Ca^{2+}, respectively. Without Ca^{2+}, a weak and long-range repulsive force commences from ca. 150 nm, increases slowly and is followed by a jump-to-contact at a final distance of -0.5 ± 0.5 nm, corresponding to mica-mica contact in water[41]. The long-range repulsion originates from double layer electrostatic repulsion, similar to normal force profiles across purified water with no added salt, decaying exponentially with surface separation D with a decay length κ^{-1} (Debye screening length) = 50 nm, close to that with water in our experiments (κ^{-1} = 70 nm) and to earlier studies across water.[41] At close separations, van der Waals attraction dominates and causes the two surfaces jump into contact. As shown schematically in Figure 6, both the repulsive profile which resembles that of pure water, and the final contact separation, clearly indicates no adsorption of the egg SM-SUVs on the mica, which we attribute to electrostatic repulsion between them.

Adding Ca^{2+} dramatically changes the normal force profiles, where monotonically increased repulsive force was observed. Onset of monotonically repulsive forces as the surfaces approach shifts to a shorter distance of 65 ± 7 nm. The repulsive force grows slowly as surface separation decreases down to ~ 20 nm, and then increases approximately exponentially until the highest applied load (corresponding to a mean contact stress P = 9.1 ± 0.7 MPa). The final "hard-wall" distance at the highest load is either 18.3 ± 1.9, 14.2 ± 0.8, or 9.5 ± 0.8 nm (Figure 4, inset), equivalent to the thickness of four, three, or two egg SM bilayers under compression.[27, 42]

After replacing 0.3 mM egg SM-SUVs dispersion in 0.03 mM Ca^{2+} with pure water, no significant change in normal force curves was observed (Figure 4, blue symbols). In addition, there was no obvious difference in normal force profiles at separation distance more than ca. 25 nm between the first and subsequent approaches (Figure 4). This is probably because of the weak repulsion between egg SM-SUVs prevents egg SM-SUVs from adhering on the bottom layer. Clearly, the adsorption of egg SM- SUVs/bilayers on mica by calcium is irreversible in water, and the gel-state boundary layers are robust and stable enough to sustain high normal load and shear (discussed below).

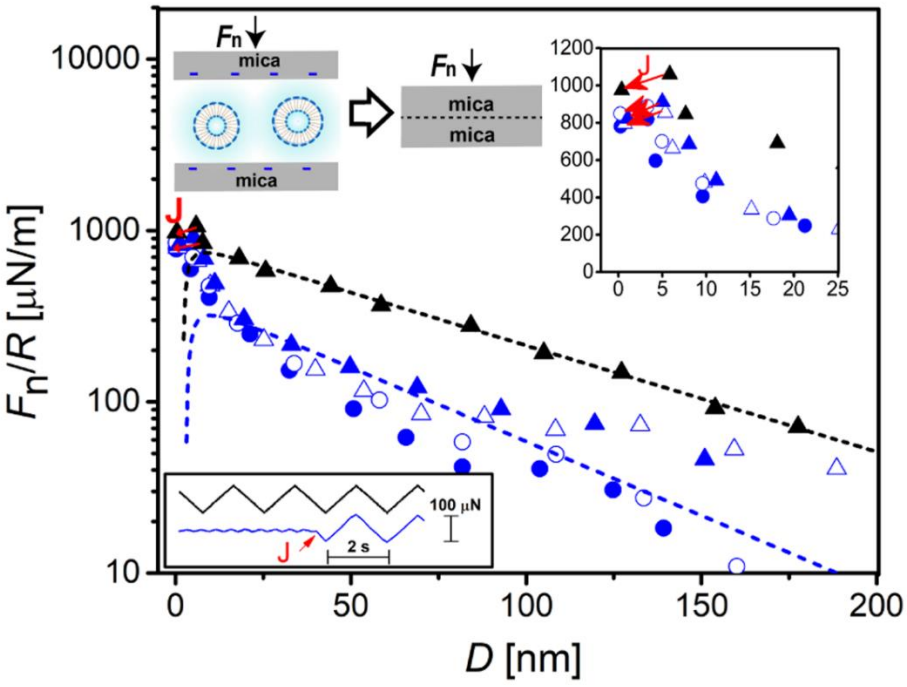

Figure 3. Normal force profiles versus surface separation distance between curved mica surfaces (F_n/R vs. D) across water (black) and 0.3 mM egg SM-SUVs in water (blue). The dash lines are fits to a Derjaguin-Landau-Verwey-Overbeek (DLVO) expression,[43, 44] $F_n/R=128\pi ck_BT\kappa^{-1}\tanh^2(e\psi_0/4k_BT)\exp(-\kappa D) - A_H/6D^2$, where c is the number concentration of electrolyte, k_B is Boltzmann constant, T is the temperature (298.2 K), and $A_H = 2\times10^{-20}$ J is the Hamaker constant value corresponding to mica-mica across water. The fitted Debye length κ^{-1} is 70 and 50 nm corresponding to an effective concentration of 1:1 electrolyte

1.9×10^{-5} and 3.7×10^{-5} M across water and SUVs, respectively. The arrows indicate that the two surfaces jump into contact, and as they do so at the point *J* they become rigidly-coupled and move in lockstep as the upper surface is moved laterally (lower inset). The lower inset shows the applied motion by PZT (upper trace) and the recorded shear force between two surfaces (lower trace) across 0.3 mM egg SM-SUV dispersion. (For interpretation of the references to color in this figure legend, the reader is referred to the web version of this article.)

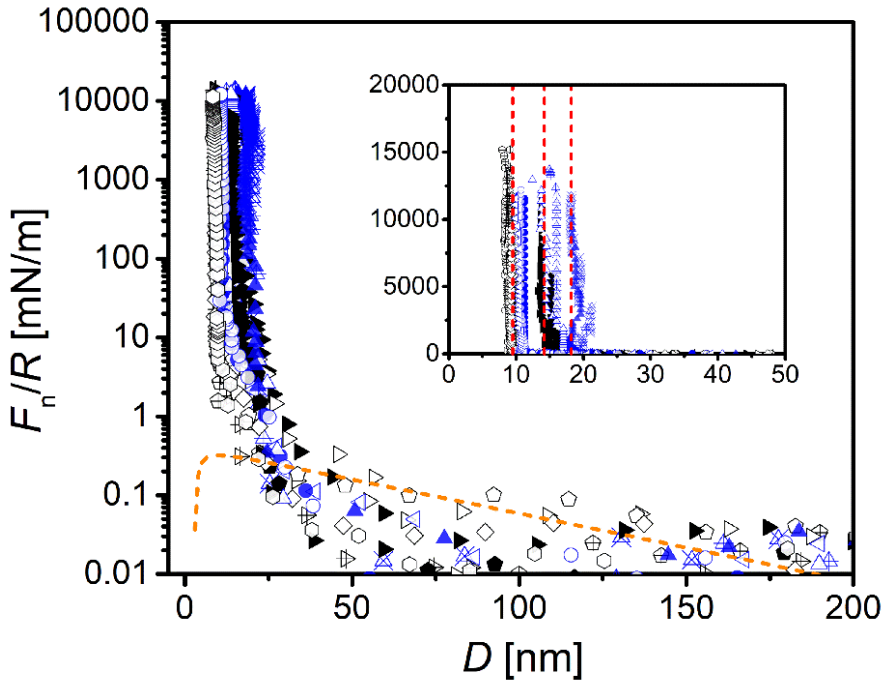

Figure 4. Normal force profiles versus surface separation distance between curved mica surfaces (F_n/R vs. D) measured after adding 0.03 mM $Ca(NO_3)_2$ (black symbols) to the egg SM-SUV dispersion of Figure 3, and after subsequently rinsing with pure water (blue symbols). Full and open symbols represent the first and subsequent approaches, while the crossed symbols represent the receding profiles. The inset shows the normal force profiles in linear scale and the vertical broken lines indicate the "hard-wall" thicknesses at 9.5, 14.2, and 18.3 nm, respectively. (For interpretation of the references to color in this figure legend, the reader is referred to the web version of this article.)

When the SM-SUVs are prepared in physiologically high salt concentration, 150 mM $NaNO_3$, and then the surface forces are measured across a similarly-high-salt solution, as seen in Figure 5, monotonic repulsion (> 0.05 mN/m) sets on at 70 ± 10 nm and the final "hard-wall" thickness is 10.3 ± 1.1 or 16.2 ± 1.0 nm at the highest compressions (Figure 5, inset), corresponding to mean contact stress P = 7.6 ± 0.8 MPa. Relatively higher repulsive forces were observed for the first approaches (filled symbols) than for the following ones (open symbols), possibly due to removal of loosely-attached material following shear on first approach.

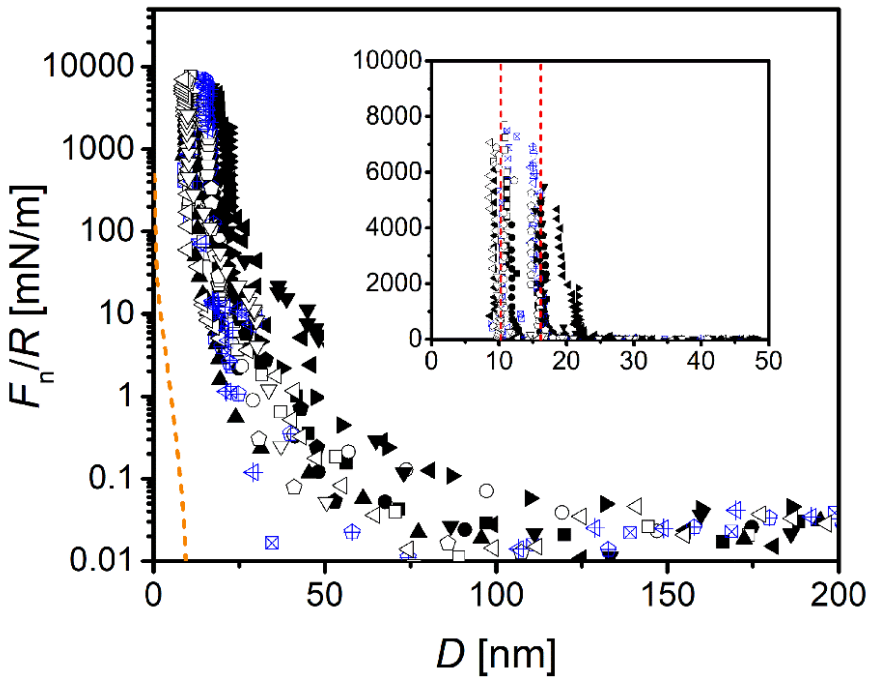

Figure 5. Normal force profiles versus surface separation distance between curved mica surfaces (F_n/R vs. D) across 0.3 mM egg SM-SUVs dispersion in 150 mM $NaNO_3$. The filled and open black symbols represent the first and subsequent approaches, and the crossed symbols are measured upon receding. The orange broken line indicates the DLVO forces (electrostatic and van der Waals forces) together with hydration force based on earlier studies between mica surfaces across high concentration salt solution (100 mM

$NaNO_3$), $F_n/R = 128\pi c k_B T \kappa^{-1} \tanh^2(e\psi_0/4k_BT)\exp(-\kappa D) - A_H/6D^2 + 2\pi E_h \exp(-D/D_h)$,[45] where the fitting parameters, including the effective (large-separation) surface potential ψ_0 = 70 mV, Debye length κ^{-1} = 1.36 nm, E_h = 0.23 J m^{-2}, and D_h = 0.2 nm are adapted from Ref. 41. The Hamaker constant value $A_H = 2\times10^{-20}$ J corresponds to mica-mica across water. Inset shows linear plot of the normal force profiles, where the vertical broken lines indicate the "hard-wall" thicknesses at 10.3 and 16.2 nm (from left to right).

In summary, the approaching force profiles between opposing egg SM layers, both in low-concentration Ca^{2+}, in water, and across high-concentration $NaNO_3$ solution, are characterized by monotonically increased repulsive forces: weak long-ranged repulsion followed by strong short-ranged repulsion at closer contact. Since surface charges of the egg SM vesicles are mostly neutralized by Ca^{2+} in water and screened in high concentration $NaNO_3$, the electrostatic repulsive force is negligible or of very short range. Therefore, the relatively long-ranged weak repulsion is attributed to steric repulsion between the adsorbed egg SM-SUVs. Similar observations have been reported for normal force profiles across PC-SUVs under water[10,11] and under high concentration monovalent salt[46]. On closer approach where the two mica surfaces were separated by two or four egg SM bilayers, the repulsion increases exponentially on compression of the bilayers trapped between contact area. Since egg SM headgroups are zwitterionic and highly hydrated,[19, 47] this short-ranged strong repulsion is dominated by the hydration repulsion between the opposing hydrated headgroups,[27] similar to the cases of PC lipids.[48, 49] Additionally, much weaker steric repulsive force arising from out-of-plane fluctuation of the supported bilayers[50] may also contribute to the total repulsion.

The normal force profiles shown in Figures 3–5 further confirm that slightly negatively charged egg SM-SUVs can be made to adsorb on negatively-charged mica either by low concentration of Ca^{2+} or by high concentration $NaNO_3$. The underlying mechanisms are different: divalent cations Ca^{2+} can bridge egg SM-SUVs and mica via electrostatic interaction, while high concentration monovalent electrolyte strongly screens the electrostatic repulsion between vesicles and mica (Figure 6), thereby promoting adsorption via non-specific interactions, such as van der Waals attraction.

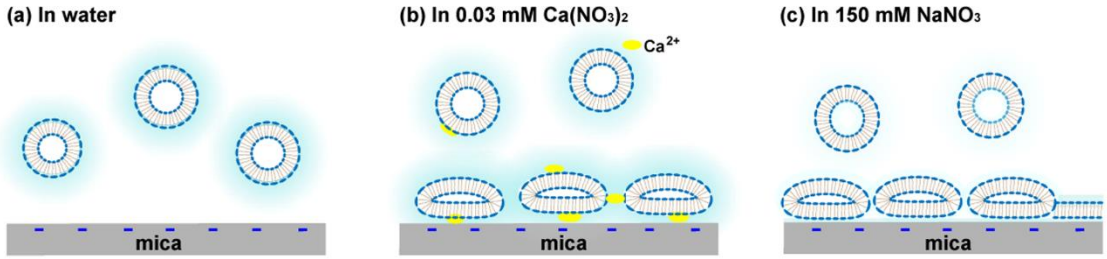

Figure 6. Schematic representation of experiments performed under different conditions. (a) Negatively charged egg SM-SUVs in water cannot adsorb on negatively-charged mica. By adding Ca^{2+} as bridge (b) or high concentration $NaNO_3$ to screen surface charge (c), egg SM-SUVs adsorb on mica in form of vesicles or bilayers, which are robust enough to sustain high normal load.

Frictional forces

Shear forces between mica surfaces coated with egg SM layers were measured along with normal forces at different separation distances. Representative shear traces as responses to the lateral back-and-forth movements of upper surface connected to PZT (indicated in Figure 1b) are shown in Figure 7.

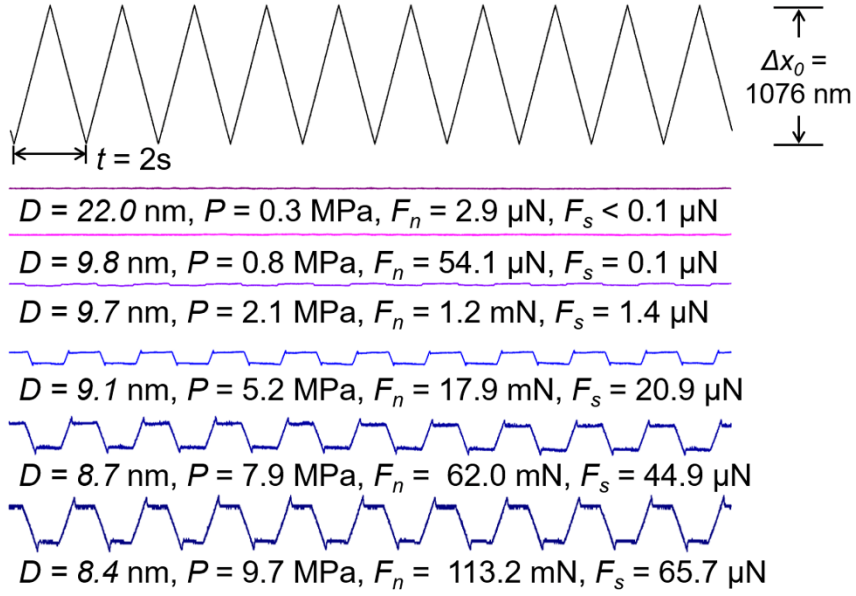

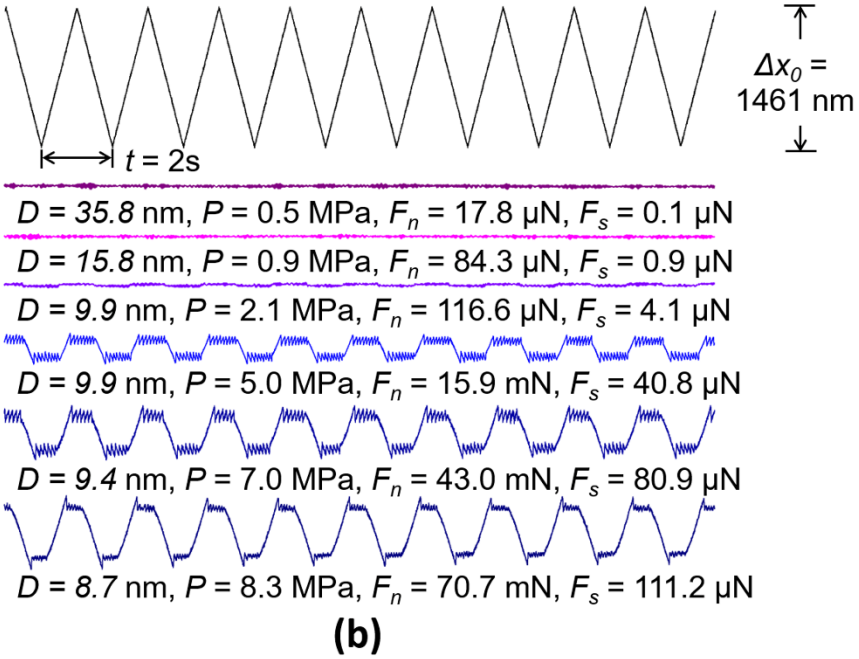

Figure 7. Typical shear traces as responses to lateral back-and-forth motion (top traces) applied to the upper surface across 0.3 mM liposome dispersion in 0.03 mM $Ca(NO_3)_2$ (a) and in 150 mM $NaNO_3$ (b). Each set of traces was recorded at the same approaching profile. As all the traces were recorded separately, their phases are not in accordance with the applied ones (top traces).

The relationship between shear force and normal load (F_s vs. F_n) is presented in Figure 8. As a general trend, F_s increases approximately linearly with F_n. Friction coefficients calculated according to $\mu = F_{s,max}/F_{n,max}$, where $F_{s,max}$ is the frictional force at the highest normal load $F_{n,max}$, are summarized in Table 1 (P_{max} is the corresponding maximal contact stress). Low friction coefficients were obtained between egg SM bilayers both in water and at physiological salt concentration. For measurements across 0.3 mM egg SM-SUVs in 0.03 mM Ca^{2+}, μ is in the range of $(7.2 \pm 1.7) \times 10^{-4}$ under pressures of 9.1 ± 0.7 MPa. After replacing with water, μ is slightly lower at $(5.3 \pm 0.8) \times 10^{-4}$ at pressures up to 9.8 ± 0.2 MPa. In 150 mM $NaNO_3$, moderately higher μ values in the range $(0.8 - 3.5) \times 10^{-3}$ at pressures ranging from 5.9 – 8.5 MPa were observed. After replacing egg SM-SUV dispersion in 150 mM $NaNO_3$ with pure water, AFM image (Figure S3) show more defects on the egg SM bilayer supported by mica, which further confirm that the high concentration monovalent salt contributes to the adsorption of slightly negatively charged vesicles.

We attribute the very low friction to the hydration lubrication mechanism acting at the slip plane between the two opposing egg SM SUVs/bilayer-coated mica surfaces, each of which exposes highly-hydrated phosphocholine headgroup layers,[51] similar to the case of lubrication between PC lipid layers.[10, 46] The somewhat higher friction coefficient observed at physiological salt concentrations may be attributed to the high concentration of ions competing with the phosphocholine headgroups for hydration water molecules, resulting in less efficient lubrication as has been previously noted at high salt concentrations.[34] Higher energy dissipation in high concentration monovalent salt than in water was reported previously on lubrication by poly(2-methacryloyloxyethyl phosphorylcholine) (pMPC)

brushes[52] and by HSPC-SUVs[46]. In addition to the dehydration effect (which reduces the efficiency of the hydration lubrication mechanism and thus leads to an increase in friction), defects on the boundary bilayer (Figure 2b) may also contribute to higher friction coefficients.[10] In the presence of 0.03 mM calcium, dehydration may also occur; but at this low salt concentration, it would be far less significant than in 150 mM $NaNO_3$. Replacing vesicle dispersion in 0.03 mM Ca^{2+} with water may also remove excess material from the boundary layer and meanwhile removes some Ca^{2+} ions which weakens the dehydration of headgroups by Ca^{2+}.[40]

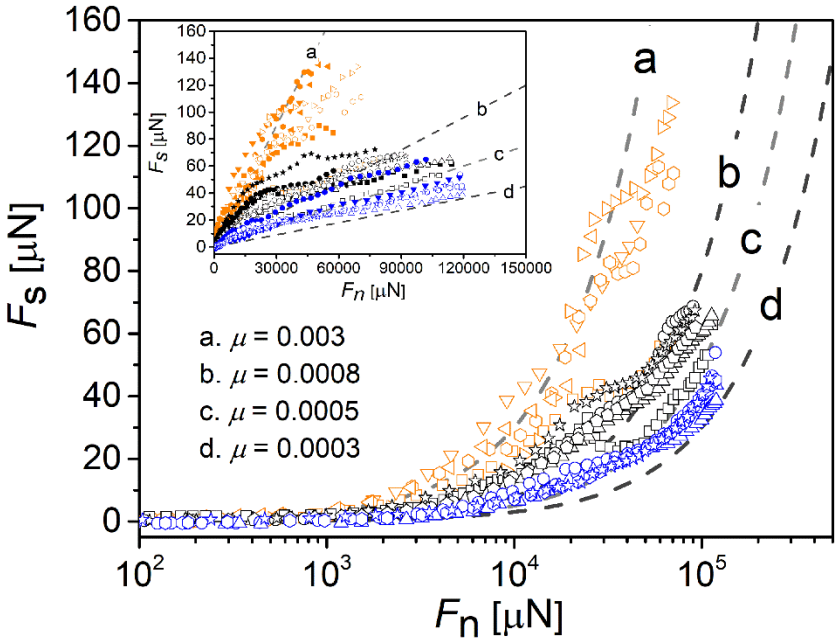

Figure 8. Shear force versus normal force (F_s vs. F_n) profiles between egg SM layers adsorbed on mica. The different-color symbols represent data obtained from measurements across 0.3 mM egg SM-SUVs in 0.03 mM $Ca(NO_3)_2$ (black); subsequent rinsing with pure water (blue); and across 0.3 mM liposome dispersion in 150 mM $NaNO_3$ (orange). The filled and open symbols display data obtained from the first and subsequent approaches. The inset shows the F_s vs. F_n profiles in linear scale. The dashed lines (a–d) indicating different friction coefficient values are used for guiding eyes. The actual friction coefficients obtained from experiments are summarized in Table 1. (For interpretation of

the references to color in this figure legend, the reader is referred to the web version of this article.)

Additionally, we also notice that the shear force values on first approaches are found to be higher than those taken from subsequent approaches at the same contact position (inset in Figure 8). This may be attributed to the high normal load and shear motion applied at the first approach, which may remove excess egg SM lipids/vesicles from the contact region, thereby reducing its roughness and resulting in reduced energy dissipation on subsequent approaches and sliding.

Table 1. Friction coefficients (μ) between egg SM SUVs/bilayers under the maximum applied pressure (P_{max})

Media	μ	P_{max}/MPa*
0.3 mM SUVs in water	Rigid-coupling**	
Adding 0.03 mM Ca^{2+}	$(7.2 \pm 1.7) \times 10^{-4}$	9.1 ± 0.7
Replacing with water	$(5.3 \pm 0.8) \times 10^{-4}$	9.8 ± 0.2
0.3 mM SUVs in 150 mM $NaNO_3$	$(2.0 \pm 0.8) \times 10^{-3}$	7.6 ± 0.8

* Egg SM SUVs/bilayers can bear higher normal pressure than P_{max}.

** Rigid coupling implies the friction force exceeds the maximal shear force that is applied in the SFB, so that the surfaces are rigidly adhered when the upper surface is made to move laterally, and no sliding occurs.

Representative shear forces at different sliding velocities (F_s vs. v) are presented in Figure 9. As v increases by 20-fold, the shear force varies to a much less extent, approximately in

the range of ± 15%. This indicates the friction reduction by the egg SM-bilayers is due to boundary lubrication under the tested conditions (both in water and at physiologically high salt concentration), where only a weak dependence of friction on sliding velocity is expected,[53] in line with what is observed.

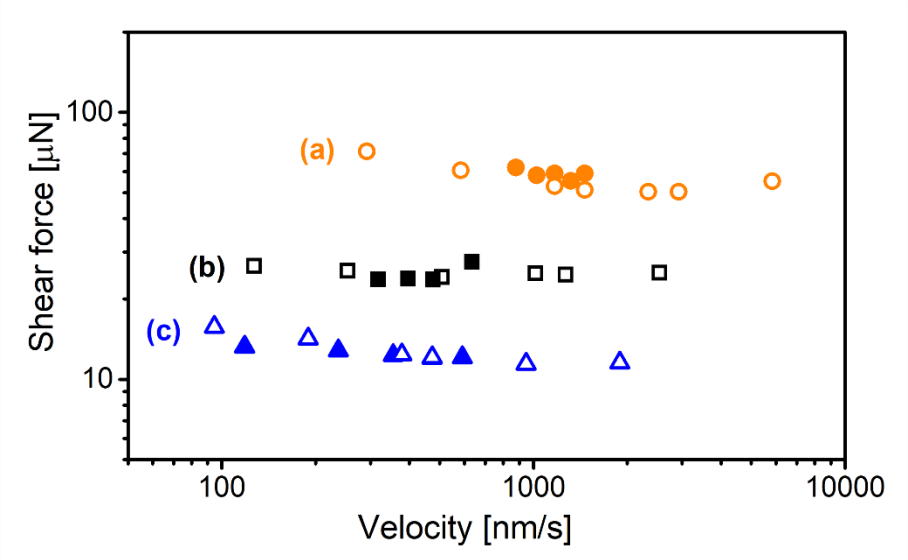

Figure 9. Representative shear forces (F_s) versus sliding velocity (v) of one surface against the other. The velocity was controlled by changing either amplitude (filled symbols) or frequency (open ones). The round (orange) symbols (a) were collected at D = 16 ± 1 nm and P = 6.7 MPa from SFB measurement across 0.3 mM egg SM-SUVs prepared and dispersed in 150 mM $NaNO_3$. The square (black) symbols (b) show data obtained at D = 15 ± 1 nm and P = 7.5 MPa, from measurements across 0.3 mM SUVs in 0.03 mM $Ca(NO_3)_2$, which was subsequently replaced by water, as in (c), triangle (blue) symbols, taken at D = 18 ± 1 nm and P = 5.2 MPa.

The extremely low friction coefficients between egg SM coated surfaces demonstrate that sphingomyelin layers are capable of excellent boundary lubrication both in water and under physiological salt concentration at pressures equivalent to biological system. It is important to emphasize that, the friction coefficient values between egg SM layers are comparable to

those for gel-state PC lipids, which have long been considered as boundary lubricants responsible for the remarkable lubrication in synovial joints. As sphingomyelin is a major component of PLs in synovial fluid and on the articular cartilage surface, it is safe to infer that SM lipids also contribute to the very efficient lubrication in biological systems, such as articular joints, up to physiologically high pressures.

Summary and Conclusions

In this study, we measured for the first time directly the normal and shear forces between egg SM layers, in the form of bilayers or vesicles, coating mica substrates, using an SFB. Two approaches were used to facilitate the adsorption of the negatively-charged egg SM-SUVs on the negatively-charged mica: one is using divalent calcium cations (0.03 mM) as a salt bridge between the egg SM and the mica; the other is screening surface charges by physiological concentration of monovalent salt. Both in the presence of low concentration Ca^{2+} or high concentration $NaNO_3$, the approaching normal force profiles are characterized by monotonic repulsion, mostly of steric origin and arising from progressive compression of egg SM vesicles on the surfaces. Extremely low friction coefficients between surface-attached egg SM layers were achieved in low concentration Ca^{2+}, pure water, and physiological salt solution, attributing to the hydration lubrication mechanism.

In summary, we have demonstrated that egg SM layers are capable of boundary lubrication at physiological pressure both in water and in physiological salt concentration, that are comparable to that seen with PC layers. Thus, we believe that, together with PC lipids, SM lipids contribute to reducing friction in lubricated biological systems, such as synovial

joints. Our finding provides insight on the biolubrication function of sphingomyelin, and may enable the design of more efficient bio-mimetic lubricants. In future work, we will focus on the other major classes of PLs in the articular joints, including phosphatidylethanolamine (PE) and negatively charged PL, before investigating more complicated biomimetic PL mixtures, including the effect of cholesterol.

Acknowledgements

This research was finally supported by the European Research Council (Advanced Grant CartiLube), by the McCutchen Foundation, by the Israel Science Foundation – National Natural Science Foundation of China joint research program (Grant 2577/17), by the Israel Ministry of Science (Grant 3-15716), and was made possible partly through the historic generosity of the Perlman Family.

Electronic supplementary information (ESI) available: DSC of egg SM-SUVs in water, size distribution and zeta potential values of egg SM-SUVs at different calcium concentrations, and morphologies of egg SM-SUVs on mica across 0.3 mM egg SM-SUV dispersion in water and after replacing 0.3 mM SUV dispersion in 150 mM $NaNO_3$ with water by AFM.

References

1. A. Erdemir; and J.-M. Martin, *Superlubricity*, Elsevier, 2007.
2. B. K. Jones, K. M. Durney, C. T. Hung and G. A. Ateshian, *J. Biomech.*, 2015, **48**, 3945-3949.
3. P. Damm, J. Dymke, R. Ackermann, A. Bender, F. Graichen, A. Halder, A. Beier and G. Bergmann, *Plos One*, 2013, **8**, e78373.
4. D. Adams and S. A. V. Swanson, *Ann Rheum Dis.*, 1985, **44**, 658-666.
5. W. A. Hodge, R. S. Fijan, K. L. Carlson, R. G. Burgess, W. H. Harris and R. W. Mann, *Proc. Natl. Acad. Sci.*, 1986, **83**, 2879-2883.
6. K. C. Morrell, W. A. Hodge, D. E. Krebs and R. W. Mann, *Proc. Nat. Acad. Sci.*, 2005, **102**, 14819-14824.
7. G. Wang, W. Huang, Q. Song and J. Liang, *Asian J. Surg.*, 2017, **40**, 463-469.
8. B. A. Hills and B. D. Butler, *Ann Rheum Dis.*, 1984, **43**, 641-648.
9. Y. Duan, Y. Liu, J. Li, S. Feng and S. Wen, *Biomacromolecules*, 2019, **20**, 1522-1529.
10. R. Sorkin, N. Kampf, L. Zhu and J. Klein, *Soft Matter*, 2016, **12**, 2773-2784.
11. R. Goldberg, A. Schroeder, G. Silbert, K. Turjeman, Y. Barenholz and J. Klein, *Adv. Mater.*, 2011, **23**, 3517-3521.
12. J. Seror, L. Zhu, R. Goldberg, A. J. Day and J. Klein, *Nat. Commun.*, 2015, **6**.
13. L. Zhu, J. Seror, A. J. Day, N. Kampf and J. Klein, *Acta Biomaterialia*, 2017, **59**, 283-292.
14. R. Sorkin, N. Kampf, Y. Dror, E. Shimoni and J. Klein, *Biomaterials*, 2013, **34**, 5465-5475.
15. A. V. Sarma, G. L. Powell and M. LaBerge, *J. Orthop. Res.*, 2001, **19**, 671-676.
16. M. K. Kosinska, G. Liebisch, G. Lochnit, J. Wilhelm, H. Klein, U. Kaesser, G. Lasczkowski, M. Rickert, G. Schmitz and J. Steinmeyer, *Arthritis Rheum.*, 2013, **65**, 2323-2333.
17. K. Simons and E. Ikonen, *Nature*, 1997, **387**, 569-572.
18. R. M. Epand, *Biophys J.*, 2003, **84**, 3102–3110.
19. B. Steinbauer, T. Mehnert and K. Beyer, *Biophys J.*, 2003, **85**, 1013-1024.
20. S. W. Chiu, S. Vasudevan, E. Jakobsson, R. J. Mashl and H. L. Scott, *Biophys J.* , 2003, **85**, 3624-3636.
21. O. Et-Thakafy, N. Delorme, F. Guyomarc'h and C. Lopez, *Chem. Phys. Lipids*, 2018, **210**, 47-59.
22. M. T. Hyvönen and P. T. Kovanen, *J. Phys. Chem. B*, 2003, **107**, 9102–9108.
23. J. P. Slotte, *BBA-Biomembranes*, 2016, **1858**, 304-310.
24. Y. A. Hannun and L. M. Obeid, *Nat. Rev. Mol. Cell Biol.*, 2008, **9**, 139-150.
25. D. A. Brown and E. London, *J. Biol. Chem.*, 2000, **275**, 17221-17224.
26. W. Tamura-Lis, L. J. Lis and J. M. Collins, *J. Colloid Interface Sci*, 1986, **114**, 214-219.
27. T. J. McIntosh, S. A. Simon, D. Needham and C. H. Huang, *Biochem.*, 2002, **31**, 2020-2024.
28. M. K. Kosinska, G. Liebisch, G. Lochnit, J. Wilhelm, H. Klein, U. Kaesser, G. Lasczkowski, M. Rickert, G. Schmitz and J. Steinmeyer, *Plos One*, 2014, **9**, e91769.
29. Avanti Polar Lipids, Inc. Home Page. Https://avantilipids.com/product/860061 (Accessed Dec 31, 2019).).
30. J. Klein and E. Kumacheva, *J. Chem. Phys.*, 1998, **108**, 6996-7009.
31. N. Jiménez-Rojo, A. B. García-Arribas, J. Sot, A. Alonso and F. M. Goñi, *BBA - Biomembranes*, 2014, **1838**, 456-464.
32. Z. Arsov, E. J. González-Ramírez, F. M. Goñi, S. Tristram-Nagle and J. F. Nagle, *Chem. Phys. Lipids*, 2018, **213**, 102-110.
33. K. P. Shaw, N. J. Brooks, J. A. Clarke, O. Ces, J. M. Seddon and R. V. Law, *Soft Matter*, 2012, **8**, 1070-1078.

34. H. I. Petrache, T. Zemb, L. Belloni and V. A. Parsegian, *Proc. Natl. Acad. Sci.*, 2006, **103**, 7982-7987.
35. R. Latorre and J. E. Hall, *Nature*, 1976, **264**, 361–363.
36. I. Dobrzyńska, J. Kotyńska, B. Szachowicz-Petelska and Z. A. Figaszewski, *Soft Matter*, 2016, **15**, 113-120.
37. Y. Tokudome, R. Uchida, T. Yokote, H. Todo, N. Hada, T. Kon, J. Yasuda, H. Hayashi, F. Hashimoto and K. Sugibayashi, *J. Liposome Res.*, 2010, **20**, 49-54.
38. F. C. Linn and L. Sokolof, *Arthritis Rheum.*, 1965, **8**, 481-494.
39. C. Redeker and W. H. Briscoe, *Langmuir*, 2019, **35**, 15739-15750.
40. R. Feng, L. Lin, Y. Li, M. Liu, Y. Guo and Z. Zhang, *Biophys. J.*, 2017, **112**, 2173-2183.
41. L. Ma, A. Gaisinskaya-Kipnis, N. Kampf and J. Klein, *Nat. Commun.*, 2015, **6**, 6060.
42. P. J. Quinn and C. Wolf, *Biochim Biophys Acta.*, 2009, **1788**, 1877-1889.
43. B. Derjaguin and L. D. Landau, *Acta Physicochimica U.R.S.S.*, 1941, **14**, 633-662.
44. E. J. W. Verwey and J. T. G. Overbeek, *Theory of the Stability of Lyophobic Colloids*, Elsevier, New York, 1948.
45. J. N. Israelachvili, *Intermolecular and Surface Forces*, Academic press, 3rd edn., 2011.
46. R. Goldberg, A. Schroeder, Y. Barenholz and J. Klein, *Biophys. J.*, 2011, **100**, 2403-2411.
47. G. G. Shipley, L. S. Avecilla and D. M. Small, *J Lipid Res.* , 1974, **15**, 124-131.
48. D. M. Leneveu, R. P. Rand and V. A. Parsegian, *Nature*, 1976, **259**, 601–603.
49. R. P. Rand and V. A. Parsegian, *BBA - Biomembranes*, 1989, **998**, 351-376.
50. P. Sharma, *Proc. Natl. Acad. Sci.* , 2013, **110**, 1976-1977.
51. T. Nyholm, M. Nylund, A. Söderholm and J. P. Slotte, *Biophys J.*, 2003, **84**, 987-997.
52. M. Chen, W. H. Briscoe, S. P. Armes and J. Klein, *Science*, 2009, **323**, 1698-1701.
53. B. Bhushan, *Introduction to Tribology*, Wiley, 2nd edn., 2013.

Supplementary Information

Normal and Shear Forces between Boundary Sphingomyelin Layers under Aqueous Conditions

Yifeng Cao, Nir Kampf, Weifeng Lin, and Jacob Klein*

Department of materials and interfaces, Weizmann Institute of Science, Rehovot 76100, Israel

*Jacob.klein@weizmann.ac.il

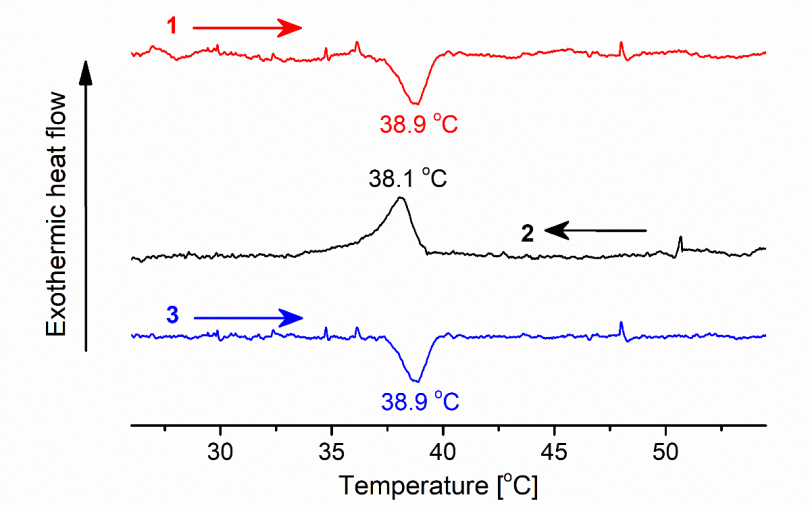

Figure S1. Differential scanning calorimetry (DSC) traces of egg SM-SUVs. DSC tests were performed on a TA Q200 differential scanning calorimeter. For the test, 35 mg of 6 mM egg SM-SUVs prepared in water was amounted into a Tezo pan and sealed. Conductivity water was used as a reference. Heating and cooling scans were controlled at 0.5 ^{o}C min^{-1}, in a temperature range of 20 - 65 ^{o}C.

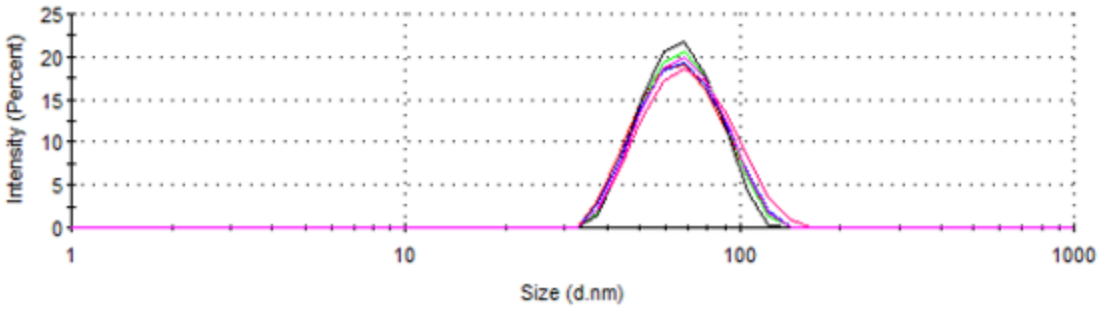

(a)

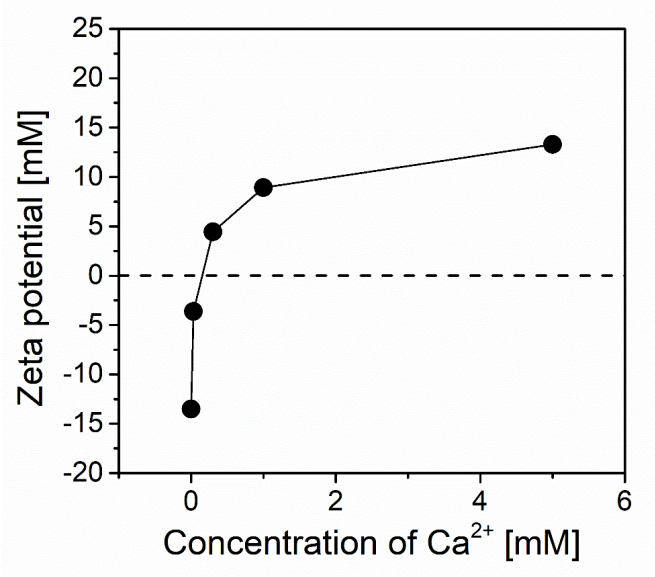

(b)

Figure S2. Size distribution (a) and zeta potential (b) at different ionic concentrations in 0.3 mM egg SM-SUV dispersion. In Figure (a), magenta and blue curves indicate liposomes prepared in water and 150 mM $NaNO_3$; pink, green, black, red curves represent dispersions in 0.03, 0.3, 1, and 5 mM $Ca(NO_3)_2$, respectively. No aggregation of SUVs was observed in the presence of 0.03 to 3 mM Ca^{2+}. In Figure (b), the filled symbols were zeta potential values measured immediately after mixing liposomes with Ca^{2+}. The zeta potential of egg SM-SUVs increases from -13.6 mM, without Ca^{2+}, increases to positive values as Ca^{2+} concentration increases to 0.3 mM, indicating that the Ca^{2+} ions adsorb to the vesicle surface and cause charge reversal.

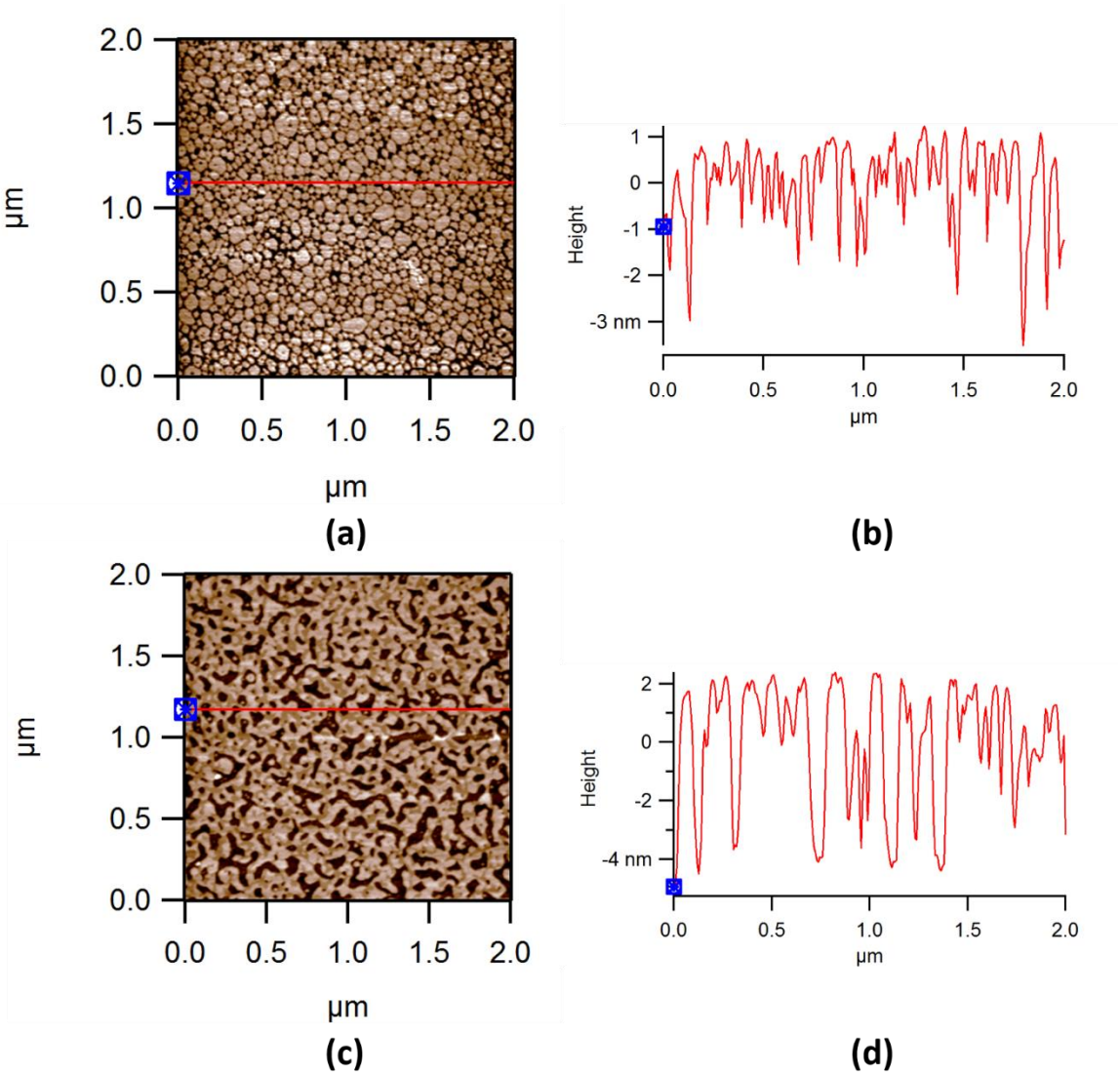

Figure S3. Morphologies of egg SM-SUVs on mica across 0.3 mM egg SM-SUV dispersion in water (a-b) and after replacing 0.3 mM SUV dispersion in 150 mM $NaNO_3$ with water (c-d) by AFM. Under 0.3 mM egg SM-SUV dispersion in water, although SFB results show few egg SM-SUVs adsorbed on mica, AFM image (a) shows egg SM patches on mica. This is possibly because the AFM tip brings liposomes to mica surface when imaging with tapping mode, which overcomes the relatively weak electrostatic repulsion and facilitates adsorption. The gap between egg SM patches indicates repulsive forces. In c-d, defects and phase separation appear on the supported egg SM bilayer, implying detachment of egg SM-bilayer from mica in water.